Engineering Analysis with Boundary Elements 33 (2009) 176–183

Contents lists available at ScienceDirect

Engineering Analysis with Boundary Elements

journal homepage: www.elsevier.com/locate/enganabound

RBF meshless method for large deflection of thin plates with immovable edges

Husain J. Al-Gahtani [a,*], Mahmoud Naffa'a [b]

[a] King Fahd University of Petroleum & Minerals (KFUMP), Dhahran 31261, Saudi Arabia
[b] Saudi Aramco, Dhahran, Saudi Arabia

ARTICLE INFO

Article history:
Received 23 July 2007
Accepted 29 May 2008
Available online 24 July 2008

Keywords:
RBF
Meshless
Meshfree
Plate
Large deflection
Immovable edge

ABSTRACT

An efficient meshless formulation is presented for large deflection of thin plates with immovable edges. In this method, a fifth-order polynomial radial basis function (RBF) is used to approximate the solution variables. The governing equations are formulated in terms of the three displacement components u, v and w. The solution is obtained by satisfying three coupled partial differential equations and their boundary conditions inside the domain and over the boundary of the plate, respectively. The collocation procedure produces a system of coupled non-linear algebraic equations, which are solved using an incremental-iterative procedure. The numerical efficiency of the proposed method is illustrated through numerical examples.

1. Introduction

In the problem of small deflection of a thin elastic plate, it is assumed that the plate is bent by lateral loads only. However, in the case of large plate deflection, the relation between external load and deflection is no longer linear. Due to large deflections, the middle plane streches, developing tensile membrane forces that may have an effect on the bending of the plate and consquently can add considerably to its load-carrying capacity. For instance, in the case of a clamped circular plate subjected to a uniform load that produces a central deflection of 100% of its thickness, the maximum stretching stress is approximately 40% of the maximum bending stress [1]. For such situations, an extended plate theory must be employed, accounting for the effect of large deflection. Large elastic deflection of a thin elastic plate is governed by coupled non-linear differential equations for which analytical solutions are available only for very few cases involving simple geometries and loading conditions [1–5]. For other cases, the problem has to be solved using numerical techniques such as the finite difference method (FDM), the finite element method (FEM) and the boundary element method (BEM). Nevertheless, the possibility of obtaining numerical solutions without resorting to the mesh-based techniques mentioned above, has been the goal of many researchers throughout the computational mechanics community for the past two decades or so. Radial basis function (RBF) is one of the most recently developed meshless methods that has attracted attention in recent years, especially in the area of computational mechanics [6–8]. This method does not require mesh generation which makes them advantageous for 3-D problems as well as problems that require frequent re-meshing such as those arising in non-linear analysis. Due to its simplicity to implement, it represents an attractive alternative to FDM, FEM and BEM as a solution method for non-linear differential equations.

The roots of RBF goes back to the early 1970s, when it was used for fitting scattered data [9]. In 1982, Nardini and Brebbia [10] combined RBF with BEM in a technique called dual reciprocity-boundary element method to solve free vibration problems, where RBF was used to transform the domain integrals into boundary integrals. Thereafter, many researchers have used RBF in conjunction with BEM to solve various problems in computational mechanics. The method, however, has not been applied directly to solve partial differential equations until 1990 by Kansa [11,12]. Since then, many researchers have suggested several variations to the original method, e.g. Refs [13–18] not to mention many others. In general, RBF method expands the solution of a problem in terms of RBFs and chooses expansion coefficients such that the governing equations and boundary conditions are satisfied at some selected domain and boundary points. However, one of the important issues in applying this technique is the determination of the proper form of RBF for a given differential equation. Most of the available RBFs involve a parameter, called shape factor. Despite the excellent results obtained by using shape-parameter dependent RBFs, their application requires a proper selection of

* Corresponding author.
E-mail address: hqatani@kfupm.edu.sa (H.J. Al-Gahtani).

0955-7997/$ - see front matter © 2008 Elsevier Ltd. All rights reserved.
doi:10.1016/j.enganabound.2008.05.004

the shape parameter to avoid instability of the solution [19,20]. In this paper, the simple fifth-order polynomial RBF that does not involve a shape factor is considered. This approach has been applied successfully to the large deflection of plates with movable edges [21]. The objective of this paper is to extend the method to plates with immovable edges. The paper is organized as follows. The governing equations based on *w–F* and *u–v–w* formulations are presented in Section 2. In Section 3, the method of collocation with RBF is illustrated, followed by the incremental-iterative procedure for solving the resulted RBF coupled non-linear equations. The efficiency of the method is demonstrated by numerical examples in Section 4, followed by some concluding remarks in Section 5.

2. Governing equations

2.1. w–F formulation

Large elastic deflection of thin elastic plates is generally governed by the two coupled non-linear differential equations, known as von Kármán equations [1], which can be expressed as:

$$\nabla^4 F = E\left[\left(\frac{\partial^2 w}{\partial x \partial y}\right)^2 - \left(\frac{\partial^2 w}{\partial x^2}\right)\left(\frac{\partial^2 w}{\partial y^2}\right)\right], \tag{1}$$

$$\nabla^4 \omega = \frac{h}{D}\left[\frac{q}{h} + \left(\frac{\partial^2 F}{\partial y^2}\right)\left(\frac{\partial^2 w}{\partial x^2}\right) + \left(\frac{\partial^2 F}{\partial x^2}\right)\left(\frac{\partial^2 w}{\partial y^2}\right) \times -2\left(\frac{\partial^2 F}{\partial x \partial y}\right)\left(\frac{\partial^2 w}{\partial x \partial y}\right)\right], \tag{2}$$

where F is a stress function, w is a displacement component perpendicular to the plane of the plate, E is the modulus of elasticity for the plate material, q is the surface loading per unit area of the plate, h is the plate thickness and $D = [(Eh^3/12(1-\nu^2))]$ is the flexural rigidity of the plate. The stress function F is related to the inplane forces through the follwong relations:

$$N_x = h\frac{\partial^2 F}{\partial y^2}, \quad N_y = h\frac{\partial^2 F}{\partial x^2}, \quad N_{xy} = -h\frac{\partial^2 F}{\partial x \partial y}. \tag{3}$$

The details for deriving Eqs. (1) and (2) are given in the classical book by Timoshenko and Woinowsky-Krieger [1]. It should be noted that the first equation represents the in-plane or membrane action while the second equation represents the transverse or bending action of the plate. Principally, there are two classes of boundary conditions, namely, movable and immovable. In the former class, the *w–F* solution approach can be readily used where the movable boundary condition is represented by $F = (\partial F/\partial n) = 0$. However, in the case of immovable edge condition $(u = v = 0)$, which is considered here, it is not possible to accurately establish the boundary conditions in terms of the stress function F. One way to overcome this difficulty is by imposing certain boundary constraints on F in an average sense [22]. The other more convenient and certainly more accurate alternative is to replace Eq. (1) by two partial differential equations in terms of the the in-plane displacements, u and v in addition to the non-linear terms involving w, as explained the following section.

2.2. u–v–w formulation

In the absence of body forces, the equations of equilibrium along x and y are given by

$$\frac{\partial N_x}{\partial x} + \frac{\partial N_{xy}}{\partial y} = 0, \tag{4}$$

$$\frac{\partial N_{xy}}{\partial x} + \frac{\partial N_y}{\partial y} = 0. \tag{5}$$

The forces acting on in the middle surface are related to the strain components through the following relations:

$$\varepsilon_x = \frac{1}{hE}(N_x - \nu N_y), \tag{6}$$

$$\varepsilon_y = \frac{1}{hE}(N_y - \nu N_x), \tag{7}$$

$$\gamma_{xy} = \frac{1}{hG}N_{xy}. \tag{8}$$

The strain components in the middle surface of the plate during bending are given by

$$\varepsilon_x = \frac{\partial u}{\partial x} + \frac{1}{2}\left(\frac{\partial w}{\partial x}\right)^2, \tag{9}$$

$$\varepsilon_y = \frac{\partial \upsilon}{\partial y} + \frac{1}{2}\left(\frac{\partial w}{\partial y}\right)^2, \tag{10}$$

$$\gamma_{xy} = \frac{\partial u}{\partial y} + \frac{\partial \upsilon}{\partial x} + \frac{\partial w}{\partial x}\frac{\partial w}{\partial y}. \tag{11}$$

Using Eqs. (9)–(11) in Eqs. (6)–(8), then in Eqs. (3)–(5), we have

$$\frac{Eh}{1-\nu^2}\left\{\frac{\partial^2 u}{\partial x^2} + \frac{\partial w}{\partial x}\frac{\partial^2 w}{\partial x^2} + \nu\left(\frac{\partial^2 \upsilon}{\partial x \partial y} + \frac{\partial^2 w}{\partial x \partial y}\frac{\partial w}{\partial y}\right) + \frac{(1-\nu)}{2}\left(\frac{\partial^2 u}{\partial y^2} + \frac{\partial^2 \upsilon}{\partial x \partial y} + \frac{\partial^2 w}{\partial x \partial y}\frac{\partial w}{\partial y} + \frac{\partial w}{\partial x}\frac{\partial^2 w}{\partial y^2}\right)\right\} = 0, \tag{12}$$

$$\frac{Eh}{1-\nu^2}\left\{\frac{(1-\nu)}{2}\left(\frac{\partial^2 u}{\partial x \partial y} + \frac{\partial^2 \upsilon}{\partial x^2} + \frac{\partial^2 w}{\partial x \partial y}\frac{\partial w}{\partial x} + \frac{\partial w}{\partial y}\frac{\partial^2 w}{\partial x^2}\right) + \frac{\partial^2 \upsilon}{\partial y^2} + \frac{\partial w}{\partial y}\frac{\partial^2 w}{\partial y^2} + \nu\left(\frac{\partial^2 u}{\partial x \partial y} + \frac{\partial w}{\partial x}\frac{\partial^2 w}{\partial x \partial y}\right)\right\} = 0. \tag{13}$$

The corresponding membrane boundary conditions are:

$$u = v = 0, \tag{14}$$

on all edges of the plate. Similarly, the terms involving F on the right hand side of Eq. (2) can be repaced by terms involving u and v, so that Eq. (2) becomes:

$$D\nabla^4 w = q + \frac{Eh}{(1-\nu^2)} \times \left\{\frac{\partial^2 w}{\partial x^2}\left[\left(\frac{\partial u}{\partial x} + \frac{1}{2}\frac{\partial w}{\partial x}\frac{\partial w}{\partial x}\right) + \nu\left(\frac{\partial \upsilon}{\partial y} + \frac{1}{2}\frac{\partial w}{\partial y}\frac{\partial w}{\partial y}\right)\right] + \frac{\partial^2 w}{\partial y^2}\left[\left(\frac{\partial \upsilon}{\partial y} + \frac{1}{2}\frac{\partial w}{\partial y}\frac{\partial w}{\partial y}\right) + \nu\left(\frac{\partial u}{\partial x} + \frac{1}{2}\frac{\partial w}{\partial x}\frac{\partial w}{\partial x}\right)\right] + (1-\nu)\frac{\partial^2 w}{\partial x \partial y}\left(\frac{\partial u}{\partial y} + \frac{\partial \upsilon}{\partial x} + \frac{\partial w}{\partial x}\frac{\partial w}{\partial y}\right)\right\}. \tag{15}$$

The transverse boundary conditions for the above equation are the same as those used for classical plate analysis, which can be written as:

$$BC_{w1}(w) = 0 \quad \text{where } BC_{w1}(w) = w \text{ or } BC_{w1}(w) = V_n, \tag{16}$$

$$BC_{w2}(w) = 0 \quad \text{where } BC_{w2}(w) = \frac{\partial w}{\partial n} \text{ or } BC_{w2}(w) = M_n, \tag{17}$$

where M_n and V_n are the normal bending moment and shear force which are given by

$$M_n = -D\left\{\nu\nabla^2 w + (1-\nu) \times \left(n_x^2\frac{\partial^2 w}{\partial x^2} + n_y^2\frac{\partial^2 w}{\partial y^2} + 2n_x n_y\frac{\partial^2 w}{\partial x\partial y}\right)\right\}, \quad (18)$$

$$V_n = -D\left\{(n_y(1-n_x^2(\nu-1)))\frac{\partial^3 w}{\partial y^3} + n_x(-2n_x^2(\nu-1)+n_y^2(\nu-1)+\nu)\frac{\partial^3 w}{\partial y^2\partial x} + n_y(n_x^2(\nu-1)-2n_y^2(\nu-1)+\nu)\frac{\partial^3 w}{\partial x^2\partial y} + n_x\left(1-n_y^2(\nu-1)\frac{\partial^3 w}{\partial x^3}\right)\right\}, \quad (19)$$

where n_x and n_y are the x and y comonents of the unit vector normal to the boundary. Eqs. (12), (13) and (15), together with their boundary conditions given by Eqs. (14), (16) and (17) represent the u–v–w formulation for large deflection of the plate.

3. RBF formulation

Consider a 2-D computational domain (Fig. 1) that represents the plate geometry. For collocation, we use node points distributed both along the boundary ($\underline{x}_B^j, j=1,\ldots,N_B$), and over the interior ($\underline{x}_D^j, j=1,\ldots,N_D$). The three displacement components are interpolated linearly by suitable RBFs:

$$u(\underline{x}) \approx \sum_{j=1}^{ND}\alpha_u^j\Phi(||\underline{x}-\underline{x}_D^j||) + \sum_{j=1}^{NB}\beta_u^j(\Phi(||\underline{x}-\underline{x}_B^j||)), \quad (20)$$

$$\upsilon(\underline{x}) \approx \sum_{j=1}^{ND}\alpha_\upsilon^j\Phi(||\underline{x}-\underline{x}_D^j||) + \sum_{j=1}^{NB}\beta_\upsilon^j(\Phi(||\underline{x}-\underline{x}_B^j||)), \quad (21)$$

$$w(\underline{x}) = \sum_{j=1}^{N_D}\alpha_w^j\Phi(||\underline{x}-\underline{x}_D^j||) + \sum_{j=1}^{N_B}\beta_w^j BC_{w1}(\Phi(||\underline{x}-\underline{x}_B^j||))\Phi + \sum_{j=1}^{N_B}\gamma_w^j BC_{w2}(\Phi(||\underline{x}-\underline{x}_B^j||)), \quad (22)$$

where $\Phi = ||\underline{x}-\underline{x}^j||^n = r^n$ is a polynomial RBF of nth degree and $\alpha_u^j, \beta_u^j, \alpha_v^j, \beta_v^j\alpha_w^j, \beta_w^j$, and γ_w^j are unknown coefficients. Unlike the other RBFs, the polynomial RBF has the important advantage of being free of a shape factor, which is a source of solution instability if not properly selected. It should be noted that there are some constraints on the permissible values of the polynomial degree n. This is explained by Table 1 that shows the results of the bi-harmonic operator ($\nabla^4\Phi$) for different degrees of the polynomial RBF. It is obvious that RBF polynomials with $n \leqslant 4$ yield either constant or singular values as $r \to 0$ and therefore these choices must be avoided. Furthermore, previous studies [13] have shown that even values of n produced inaccurate solutions. Therefore, we are left with odd values of $n \geqslant 5$. Few numerical experiments have been carried out to compare the accuracy of the solution of the linear plate problem for $n = 5$, 7 and 9. The results of these experiments have not shown any appreciable difference in terms of accuracy for $n = 5$ and 7. For $n = 9$, however, stability problems have been encountered especially for high node intensities. Therefore, it was decided to use $n = 5$. The $4N_B$+$3N_D$ unknown coefficients: $\alpha_u^j, \beta_u^j, \alpha_v^j, \beta_v^j\alpha_w^j, \beta_w^j$, and γ_w^j, can be determined by satisfying the governing equations at the N_D domain points, and by satisfying the corresponding boundary conditions at the N_B boundary points. Before doing that, let us put the governing equations (12), (13) and (15) in the following compact forms:

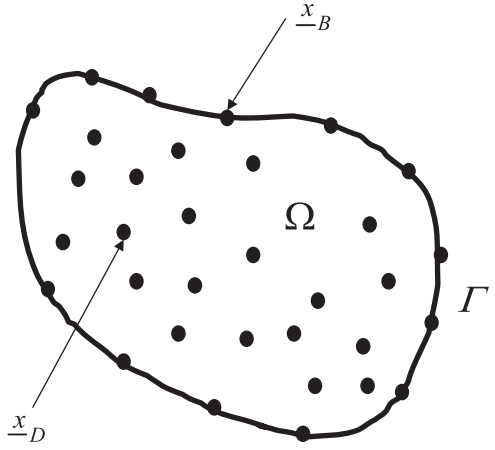

Fig. 1. Boundary and domain nodes.

Table 1
Results of the bi-harmonic operator ($\nabla^4\Phi$) for different degrees of the polynomial RBF

N	$\nabla^4\Phi$
1	$1/r^3$
2	0
3	$9/r$
4	64
5	$225r$
6	$576r^2$
7	$1225r^3$
8	$2304r^4$
9	$3969r^5$

$$L_{11}(u) + L_{12}(\upsilon) = NL_1(w), \quad (23)$$

$$L_{21}(u) + L_{22}(\upsilon) = NL_2(w), \quad (24)$$

$$D\nabla^4 w = q + NL_3(u,\upsilon,w), \quad (25)$$

where

$$L_{11}(u) = \frac{2u_{xx}+(1-\nu)u_{yy}}{2(1-\nu^2)}, \quad (26)$$

$$L_{12}(\upsilon) = \frac{\upsilon_{xy}}{2(1-\nu)}, \quad (27)$$

$$L_{21}(u) = \frac{u_{xy}}{2(1-\nu)}, \quad (28)$$

$$L_{22}(\upsilon) = \frac{2\upsilon_{yy}+(1-\nu)\upsilon_{xx}}{2(1-\nu^2)}, \quad (29)$$

$$NL_1(w) = -\frac{(1+\nu)w_{xy}w_y + w_x(2w_{xx}+(1-\nu)w_{yy})}{2(1-\nu^2)}, \quad (30)$$

$$NL_2(w) = -\frac{(1+\nu)w_x w_{xy} + w_y((1-\nu)w_{xx}+2w_{yy})}{2(1-\nu^2)}, \quad (31)$$

$$NL_3(u,\upsilon,w)=\frac{Eh}{1-\nu^2}\left\{w_{xx}\left(\left(u_x+\frac{1}{2}w_x^2\right)+\nu\left(\upsilon_y+\frac{1}{2}w_y^2\right)\right)+w_{yy}\left(\left(\upsilon_y+\frac{1}{2}w_y^2\right)+\nu\left(\upsilon_x+\frac{1}{2}w_x^2\right)\right)+(1-\nu)w_{xy}(u_y+\upsilon_x+w_xw_y)\right\}. \tag{32}$$

Applying the in-plane boundary conditions, i.e. Eqs. (20) and (21) at the N_B boundary points and the in-plane governing equations, i.e. Eqs. (23) and (24) at the N_D domain points, we have:

$$\begin{bmatrix}\Phi(x_B,x_D) & \Phi(x_B,x_B) & 0 & 0\\ 0 & 0 & \Phi(x_B,x_D) & \Phi(x_B,x_B)\\ L_{11}(\Phi(x_D,x_D)) & L_{11}(\Phi(x_D,x_B)) & L_{12}(\Phi(x_D,x_D)) & L_{12}(\Phi(x_D,x_B))\\ L_{21}(\Phi(x_D,x_D)) & L_{21}(\Phi(x_D,x_B)) & L_{22}(\Phi(x_D,x_D)) & L_{22}(\Phi(x_D,x_B))\end{bmatrix}\times\begin{bmatrix}\alpha_u\\ \beta_u\\ \alpha_\upsilon\\ \beta_\upsilon\end{bmatrix}=\begin{bmatrix}0\\ 0\\ NL_1(w)\\ NL_2(w)\end{bmatrix}. \tag{33}$$

Similarly, repeating the same procedure for the transverse boundary conditions and governing equation, we have:

$$\begin{bmatrix}BC_{w1}(\Phi(x_B,x_D)) & BC_{w1}(B_{w1}(\Phi(x_B,x_B))) & BC_{w1}(B_{w2}(\Phi(x_B,x_B)))\\ BC_{w1}(\Phi(x_B,x_D)) & BC_{w2}(BC_{w1}(\Phi(x_B,x_B))) & BC_{w2}(BC_{w2}(\Phi(x_B,x_B)))\\ D\nabla^4(\Phi(x_D,x_D)) & D\nabla^4(BC_{w1}(\Phi(x_D,x_B))) & D\nabla^4(BC_{w2}(\Phi(x_D,x_B)))\end{bmatrix}\times\begin{bmatrix}\alpha_w\\ \beta_w\\ \gamma_w\end{bmatrix}=\begin{bmatrix}0\\ 0\\ q+NL_3(u,v,w)\end{bmatrix}. \tag{34}$$

In order to solve the above coupled and highly non-linear equations, an incremental-iterative procedure is performed. In the following, the superscripts represent increments while subscripts represent iterations. As an example, the quantity $w^k_{i,xy}$ represents the second derivative of w with respect to x for the kth increment and ith iteration. Let us denote to the number of increments by n. The following steps describe the incremental-iterative procedure:

1. Apply the first load increment and set the initial values of derivatives of all u, υ and w terms (u_x, u_y, υ_x, υ_y, w_{xx}, w_{yy} and w_{xy}) to zero so that the system of Eq. (34) becomes a linear system of equations that can be solved for the first estimates of the coefficients α_w, β_w and γ_w.
2. Use the first estimates of α_w, β_w and γ_w in Eq. (22) to obtain the first estimate of the deflection w_1^1. Note that w_1^1 corresponds to the solution of small-deflection theory for the first load increment.
3. Compute $NL_1(w_1^1)$ and $NL_2(w_1^1)$, then solve Eq. (33) for the first estimates of the coefficients α_u, β_u, α_υ and β_υ.
4. Use the first estimates of α_u, β_u, α_υ and β_υ in Eqs. (20) and (21) to obtain the first estimate of the in-plane displacements, u_1^1 and υ_1^1.
5. Update the right hand side of Eq. (34) by computing $NL_3(u_1^1,\upsilon_1^1,w_1^1)$.
6. Use Eq. (22) to obtain the second estimate of the deflection w_2^1 and compute $NL_1(w_2^1)$ and $NL_2(w_2^1)$.
7. Repeat the above steps until convergence is achieved, otherwise, decrease the load increment and repeat the iterations.
8. Add the second load increment and use the values obtained for $NL_3(u_n^1,\upsilon_n^1,w_n^1)$ at the last iteration of the first load increment, then repeat the above iterative procedure.
9. Continue adding increments until the total load is applied.

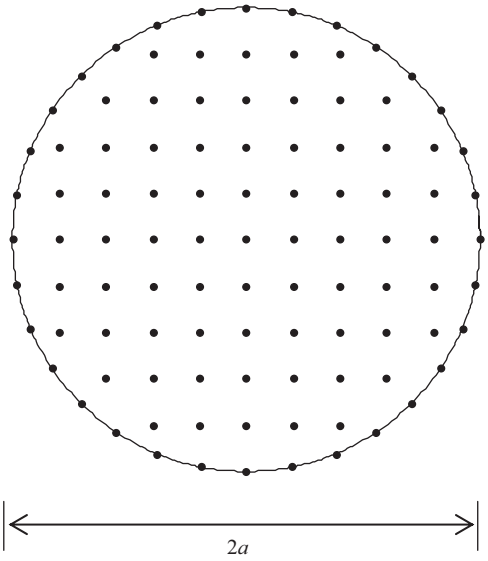

Fig. 2. Boundary and domain node distribution for Example 1 ($N_B = 32$; $N_D = 69$).

4. Numerical examples

In order to examine the effectiveness of the proposed RBF method for large deflection of thin plates, the following three examples are considered. The accuracy of RBF solutions are compared with the FEM solutions by calculating the % absolute relative differences. All FEM solutions are obtained using the package ANSYS 9.0 [23] by employing the eight-node structural shell element named *SHELL93* that has large deflection capability. In all examples, the load is assumed to be uniformly distributed = q, Poisson ratio ν is assumed 0.3. For generality of the solutions, all quantities are made dimensionless, so that the coordinates, the load, the deflection and the stress are represented by $\bar{x}=x/a$, $\bar{y}=y/a$, $\bar{q}=qa^4/Eh^4$, $\bar{w}=w/h$ and $\bar{\sigma}=\sigma a^2/Eh^2$, respectively. As a first example, let us consider a simply supported circular plate of radius = a with immovable boundary subjected to a uniform load $\bar{q}$, where $0.125\leqslant\bar{q}\leqslant2.0$. A uniform node distribution consisting of 32 boundary nodes and 69 domain nodes according to Fig. 2 has been used. An approximate analytical solution for the problem is available [1] which can be expressed in terms of dimensionless quantities as follows:

$$\bar{w}_c+A\bar{w}_c^3=B\bar{q}, \tag{35}$$

$$\bar{\sigma}_m=\alpha\bar{w}_c^2, \tag{36}$$

$$\bar{\sigma}_b=\beta\bar{w}_c^2, \tag{37}$$

where $\bar{w}_c$ is the central deflection, $\bar{\sigma}_m$ the stress in the plate middle plane (membrane stress) and $\bar{\sigma}_b$ the extreme fiber bending stress. The constants are $A=1.852$, $B=0{:}696$, $\alpha=0.905$ and $\beta=1.778$. The evolution of the plate maximum deflection at its center with the applied load is presented in Table 2, which reveals a very close agreement among RBF, FEM and the analytical solutions. Similar conclusion can be said about the results for membrane and bending stresses given in Table 3. The analytical solution for locations other than the center of the plate is not available and therefore, the variations of the deflection $\bar{w}$, the radial membrane stress $\bar{\sigma}_m$, and the radial bending stress $\bar{\sigma}_b$ due to the maximum load $\bar{q}=2.0$ as obtained by FEM and RBF are given in Table 4. Once again the RBF solutions for the deflection and stresses compare very well with the FEM solutions with a maximum relative difference of 4.90% for the bending stress at

$r/a = 0.9$ when the plate is subjected to the maximum load of 2.0. As a second example, let us consider a clamped a by a square plate with immovable boundary conditions subjected to a uniform load $\bar{q}$, where $3.67 \leqslant \bar{q} \leqslant 88$. Exact solution does not exist for this problem and therefore, comparison is made with FEM solution only. A node distribution consisting of 36 boundary nodes and 81 domain nodes (Fig. 3) has been used. The load has been increased with equal increments of 3.67 until the total load has been applied. Table 5 shows the deflection $\bar{w}$, the membrane stress $\bar{\sigma}_m$ and the bending stress $\bar{\sigma}_b$ computed at the center of the plate for different load increments. Comparing the RBF results with the

Table 2
Maximum (central) deflection $\bar{w}$ versus load $\bar{q}$

$\bar{q}$	$\bar{w}$			
	Analytical	FEM	RBF	%Error[a]
0.125	0.08583	0.0856	0.0867	1.2850
0.25	0.1656	0.1651	0.167	1.1508
0.375	0.2365	0.2357	0.2379	0.9334
0.5	0.2987	0.2974	0.2997	0.7734
0.625	0.3533	0.3515	0.3537	0.6259
0.75	0.4018	0.3993	0.4015	0.5510
0.875	0.4454	0.4421	0.4442	0.4750
1.0	0.4849	0.4808	0.4828	0.4160
1.125	0.521	0.5161	0.5181	0.3875
1.25	0.5544	0.5487	0.5503	0.2916
1.375	0.5854	0.5788	0.5806	0.3110
1.5	0.6144	0.6069	0.6087	0.2966
1.625	0.6417	0.6333	0.6334	0.0158
1.75	0.6674	0.658	0.6645	0.9878
1.875	0.6918	0.6816	0.6852	0.5282
2.0	0.7150	0.7049	0.703	0.2695

[a] $|(\text{RBF}-\text{FEM})/\text{FEM})| \times 100$.

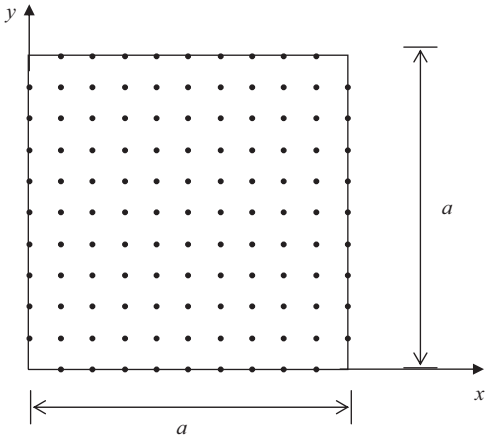

Fig. 3. Boundary and domain node distribution for Example 2 ($N_B = 36$; $N_D = 81$).

Table 3
Membrane and bending stresses at the center of the plate vs. load $\bar{q}$

$\bar{q}$	$\bar{\sigma}_m$				$\bar{\sigma}_b$			
	Analytical	FEM	RBF	%Error	Analytical	FEM	RBF	%Error
0.125	0.0067	0.00667	0.00683	2.3988	0.1526	0.1526	0.1537	0.7208
0.25	0.02482	0.0248	0.02534	2.1774	0.2944	0.2935	0.295	0.5111
0.375	0.0506	0.0504	0.05146	2.1032	0.4205	0.4175	0.4187	0.2874
0.5	0.0807	0.0804	0.08174	1.6667	0.531	0.5244	0.525	0.1144
0.625	0.113	0.1124	0.114	1.4235	0.6282	0.6168	0.6167	0.0162
0.75	0.1461	0.1452	0.147	1.2397	0.7145	0.6974	0.6966	0.1147
0.875	0.1795	0.1782	0.18	1.0101	0.7919	0.7686	0.7671	0.1952
1.0	0.2128	0.211	0.2128	0.8531	0.8621	0.832	0.8298	0.2644
1.125	0.2457	0.2434	0.2453	0.7806	0.9264	0.8893	0.8866	0.3036
1.25	0.2782	0.2752	0.2769	0.6177	0.9857	0.9413	0.9377	0.3824
1.375	0.3102	0.3066	0.3086	0.6523	1.0409	0.9889	0.9853	0.3640
1.5	0.3417	0.3374	0.3387	0.3853	1.0924	1.0329	1.0287	0.4066
1.625	0.3726	0.3674	0.3696	0.5988	1.1409	1.0737	1.0663	0.6892
1.75	0.4031	0.3972	0.3998	0.6546	1.1867	1.1117	1.1153	0.3238
1.875	0.4331	0.426	0.4292	0.7512	1.23	1.1189	1.1423	2.0913
2.0	0.4627	0.455	0.457	0.4396	1.2713	1.1261	1.1701	3.9073

Table 4
Distribution of deflection and stresses along the radial direction ($\bar{q} = 2.0$)

r/a	$\bar{w}$			$\bar{\sigma}_m$			$\bar{\sigma}_b$		
	FEM	RBF	%Error	FEM	RBF	%Error	FEM	RBF	%Error
0.0	0.7049	0.703	0.2695	0.455	0.457	0.4396	1.1261	1.1701	3.9073
0.1	0.6964	0.6948	0.2298	0.4534	0.4552	0.3970	1.1707	1.1646	0.5211
0.2	0.6719	0.6704	0.2232	0.4489	0.4498	0.2005	1.1515	1.1454	0.5297
0.3	0.6311	0.6299	0.1901	0.4397	0.4410	0.2957	1.1158	1.1110	0.4302
0.4	0.5751	0.5742	0.1565	0.4286	0.4289	0.0700	1.0614	1.0581	0.3109
0.5	0.5048	0.5039	0.1783	0.4147	0.4139	0.1929	0.9839	0.9819	0.2033
0.6	0.4208	0.4204	0.0951	0.3982	0.3962	0.5023	0.8766	0.8765	0.0114
0.7	0.3257	0.3256	0.0307	0.3795	0.3766	0.7642	0.7323	0.7350	0.3687
0.8	0.2217	0.2216	0.0451	0.3588	0.3533	1.5329	0.5448	0.5502	0.9912
0.9	0.1117	0.1118	0.0895	0.3032	0.3138	3.4960	0.337	0.3205	4.8961

Table 5
Deflection and stresses at the center of plate vs. load $\bar{q}$

$\bar{q}$	$\bar{w}$			$\bar{\sigma}_m$			$\bar{\sigma}_b$		
	FEM	RBF	%Error	FEM	RBF	%Error	FEM	RBF	%Error
3.67	0.0506	0.0503	0.5929	0.00850	0.00842	0.9412	0.504	0.5016	0.4762
7.33	0.1008	0.1002	0.5952	0.0337	0.0334	0.8902	1.0028	0.998	0.4787
11.00	0.1502	0.1493	0.5992	0.0749	0.0742	0.9346	1.4915	1.4844	0.4760
14.67	0.1985	0.1974	0.5542	0.1308	0.1295	0.9939	1.966	1.9569	0.4629
18.33	0.2455	0.2441	0.5703	0.2000	0.198	1.0000	2.4232	2.4124	0.4457
22.00	0.2910	0.2894	0.5498	0.2806	0.278	0.9266	2.8608	2.8485	0.4299
25.67	0.3349	0.3331	0.5375	0.3713	0.3679	0.9157	3.2776	3.2641	0.4119
29.33	0.3771	0.3751	0.5304	0.4705	0.4662	0.9139	3.6731	3.6586	0.3948
33.00	0.4177	0.4154	0.5506	0.5766	0.5713	0.9192	4.0473	4.032	0.3780
36.67	0.4566	0.4542	0.5256	0.6884	0.6821	0.9152	4.4009	4.385	0.3613
40.33	0.4939	0.4913	0.5264	0.8045	0.7975	0.8701	4.7345	4.7182	0.3443
44.00	0.5297	0.5270	0.5097	0.9247	0.9165	0.8868	5.0492	5.0327	0.3268
47.67	0.5641	0.5612	0.5141	1.0473	1.0383	0.8594	5.3462	5.3296	0.3105
51.33	0.597	0.5941	0.4858	1.1723	1.1623	0.8530	5.6265	5.61	0.2933
55.00	0.6287	0.6257	0.4772	1.2988	1.2878	0.8469	5.8913	5.8749	0.2784
58.67	0.6592	0.6560	0.4854	1.4265	1.4145	0.8412	6.1415	6.1255	0.2605
62.33	0.6886	0.6853	0.4792	1.5549	1.542	0.8296	6.3786	6.3629	0.2461
66.00	0.7169	0.7135	0.4743	1.6838	1.6699	0.8255	6.6031	6.5879	0.2302
69.67	0.7442	0.7407	0.4703	1.8130	1.798	0.8274	6.8161	6.8014	0.2157
73.33	0.7705	0.7670	0.4543	1.9421	1.9262	0.8187	7.0188	7.0044	0.2052
77.00	0.796	0.7924	0.4523	2.0711	2.0542	0.8160	7.2113	7.1975	0.1914
80.67	0.8207	0.8170	0.4508	2.1997	2.1819	0.8092	7.3944	7.3815	0.1745
84.33	0.8446	0.8409	0.4381	2.3279	2.309	0.8119	7.5695	7.5571	0.1638
88.00	0.8678	0.864	0.4379	2.4555	2.436	0.7941	7.7364	7.7247	0.1512

Table 6
Distribution of deflection and stresses (at $y = 0.5$) for $\bar{q} = 88$

x/a	$\bar{w}$			$\bar{\sigma}_m$			$\bar{\sigma}_b$		
	FEM	RBF	%Error	FEM	RBF	%Error	FEM	RBF	%Error
0.05	0.043	0.0409	4.8837	1.9703	1.9192	2.5935	−12.692	−13.1659	3.7338
0.1	0.1451	0.142	2.1365	2.0602	2.0394	1.0096	−5.764	−5.874	1.9084
0.15	0.2754	0.2719	1.2709	2.1404	2.109	1.4670	−0.8577	−0.8734	1.8305
0.2	0.4126	0.4089	0.8968	2.2145	2.1883	1.1831	2.521	2.484	1.4677
0.25	0.5424	0.5387	0.6822	2.2821	2.2571	1.0955	4.7606	4.7357	0.5230
0.3	0.6558	0.652	0.5794	2.3412	2.3187	0.9610	6.1725	6.1544	0.2932
0.35	0.7473	0.7435	0.5085	2.3899	2.3686	0.8913	7.007	6.9926	0.2055
0.4	0.8139	0.8101	0.4669	2.4259	2.4057	0.8327	7.4604	7.4477	0.1702
0.45	0.8543	0.8505	0.4448	2.4481	2.4283	0.8088	7.6747	7.6628	0.1551
0.5	0.8678	0.864	0.4379	2.4555	2.436	0.7941	7.7364	7.7247	0.1512

corresponding ones obtained by FEM shows that they are in a very good agreement. In Table 6, the profiles for deflection and stresses at $y = 0.5a$ under the maximum load $\bar{q} = 88$ are given. Note that values for $0.5 \leqslant x/a \leqslant 1.0$ are reflections of values $0.0 \leqslant x/a \leqslant 0.5$ and therefore, they are not included in the table. The maximum error for this problem is 4.88% for the displacement near the boundary at $x/a = 0.05$. As a last example, let us repeat the above problem by assuming simply supported edges for the plate. Exact solution does not exist for this problem, either, and therefore, comparison is made with FEM solution only. The load has been increased with equal increments of 1.375 until the total load has been applied. Table 7 shows the deflection $\bar{w}$, the membrane stress $\bar{\sigma}_m$ and the bending stress $\bar{\sigma}_b$ computed at the center of the plate for different load increments, while Table 8 gives the profiles for deflection and stresses at $y = 0.5a$ under the maximum load $\bar{q} = 33$. Once again, both tables show very good agreements between RBF and the FEM solutions with a maximum relative error of 4.77% occurring for the bending stress at $x/a = 0.05$. It should be noted that the maximum errors for all the three examples occur for solutions near the boundary.

5. Conclusions

This work is an extension of the previous work on the use of RBF for large deflection of thin plates. The current paper addresses the case of plates having immovable edges. The method presented here is based on the use of a fifth-order polynomial RBF to build approximations of the three components of the plate displacement. The solution is obtained by collocating the governing and boundary conditions equations at some selected points on the boundary and inside the domain. The employed polynomial RBF does not require a shape parameter, which makes it more efficient than other RBFs. Furthermore, the method can be easily extended to other non-linear problems.

Table 7
Deflection and stresses at the center of plate vs. load $\bar{q}$

$\bar{q}$	$\bar{w}$			$\bar{\sigma}_m$			$\bar{\sigma}_b$		
	FEM	RBF	%Error	FEM	RBF	%Error	FEM	RBF	%Error
1.375	0.0606	0.0607	0.1650	0.0112	0.0112	0.0000	0.3931	0.3925	0.1526
2.750	0.1195	0.1195	0.0000	0.0435	0.0435	0.0000	0.7734	0.772	0.1810
4.125	0.1753	0.1752	0.0570	0.0937	0.0936	0.1067	1.1315	1.1291	0.2121
5.500	0.2272	0.227	0.0880	0.1574	0.1572	0.1271	1.4623	1.4648	0.1710
6.875	0.2752	0.2748	0.1453	0.2311	0.2305	0.2596	1.765	1.7653	0.0170
8.250	0.3194	0.3188	0.1879	0.3113	0.3103	0.3212	2.0407	2.0384	0.1127
9.625	0.36	0.3594	0.1667	0.396	0.3944	0.4040	2.2919	2.2868	0.2225
11.000	0.3977	0.3968	0.2263	0.4833	0.481	0.4759	2.5212	2.5134	0.3094
12.375	0.4326	0.4314	0.2774	0.572	0.569	0.5245	2.7315	2.7212	0.3771
13.750	0.465	0.4648	0.0430	0.6614	0.6625	0.1663	2.9249	2.9124	0.4274
15.125	0.4954	0.4947	0.1413	0.7508	0.7508	0.0000	3.1037	3.0893	0.4640
16.500	0.5238	0.5227	0.2100	0.84	0.8388	0.1429	3.2696	3.2536	0.4894
17.875	0.5507	0.5492	0.2724	0.9287	0.9261	0.2800	3.4243	3.407	0.5052
19.250	0.576	0.5741	0.3299	1.0166	1.0127	0.3836	3.5691	3.5505	0.5211
20.625	0.6	0.5978	0.3667	1.1038	1.0983	0.4983	3.7049	3.6935	0.3077
22.000	0.6229	0.6203	0.4174	1.19	1.1831	0.5798	3.8328	3.8212	0.3027
23.375	0.6447	0.6417	0.4653	1.2753	1.2669	0.6587	3.9537	3.9331	0.5210
24.750	0.6656	0.6623	0.4958	1.3596	1.3498	0.7208	4.0683	4.0473	0.5162
26.125	0.6855	0.6819	0.5252	1.4431	1.4319	0.7761	4.177	4.1559	0.5051
27.500	0.7047	0.702	0.3831	1.5255	1.5139	0.7604	4.2805	4.2686	0.2780
28.875	0.7231	0.7189	0.5808	1.607	1.5941	0.8027	4.3793	4.3688	0.2398
30.250	0.7409	0.7364	0.6074	1.669	1.6717	0.1618	4.4552	4.4526	0.0584
31.625	0.758	0.7533	0.6201	1.7672	1.7533	0.7866	4.5641	4.5434	0.4535
33.000	0.7746	0.7695	0.6584	1.8461	1.8295	0.8992	4.6509	4.6263	0.5289

Table 8
Distribution of deflection and stresses (at $y = 0.5$) for $\bar{q} = 33.0$

x/a	$\bar{w}$			$\bar{\sigma}_m$			$\bar{\sigma}_b$		
	FEM	RBF	%Error	FEM	RBF	%Error	FEM	RBF	%Error
0.05	0.1331	0.1316	1.1270	1.9535	1.9242	1.4999	1.5006	1.382	**4.7714**
0.1	0.2603	0.2578	0.9604	1.9579	1.9265	1.6038	2.5985	2.5254	2.8132
0.15	0.3773	0.3741	0.8481	1.9501	1.9218	1.4512	3.3791	3.3274	1.5300
0.2	0.4813	0.4776	0.7688	1.9345	1.9081	1.3647	3.9114	3.8721	1.0048
0.25	0.5706	0.5664	0.7361	1.9145	1.8908	1.2379	4.2545	4.2226	0.7498
0.3	0.644	0.6395	0.6988	1.8935	1.8721	1.1302	4.4599	4.432	0.6256
0.35	0.7012	0.6965	0.6703	1.8744	1.855	1.0350	4.5715	4.5456	0.5666
0.4	0.742	0.7371	0.6604	1.8592	1.8413	0.9628	4.6246	4.5996	0.5406
0.45	0.7664	0.7614	0.6524	1.8494	1.8325	0.9138	4.6457	4.621	0.5317
0.5	0.7746	0.7695	0.6584	1.8461	1.8295	0.8992	4.6509	4.6263	0.5289

Acknowledgment

The first author would like to express his appreciation to King Fahd University of Petroleum & Minerals for supporting this study.

References

[1] Timoshenko SP, Woinowsky-Kreiger S. Theory of plates and shells. New York: McGraw-Hill; 1959.
[2] Augural C. Stresses in plates and shells. New York: McGraw-Hill; 1999.
[3] Little GH. Efficient large deflection analysis of rectangular plates with general transverse form of displacement. Comput Struct 1999;71(3):333–52.
[4] Little GH. Large deflections of rectangular plates with transverse edges remaining straight. Comput Struct 1999;71(3):353–7.
[5] Ramachandra LS, Roy D. A novel technique in the solution of axisymmetric large deflection analysis of a circular plate. J Appl Mech 2001;68(5):814–6.
[6] Chen JT, Chen IL, Chen KH, Lee YT, Yeh YT. A meshless method for free vibration analysis of circular and rectangular clamped plates using radial basis function. Eng Anal Bound Elements 2004;28(5):535–45.
[7] Liew KL, Chen XL, Reddy JN. Mesh-free radial basis function method for buckling analysis of non-uniformly loaded arbitrarily shaped shear deformable plates. Comput Meth Appl Mech Eng 2004;193(3):205–24.
[8] Tiago CM, Leitão VMA. Application of radial basis functions to linear and nonlinear structural analysis problems. Comput Math Appl 2006;51(8):1311–34.
[9] Hardy RL. Multiquadric equations of topography and other irregular surfaces. Geophys Res 1971;176:1905–15.
[10] Nardini D, Brebbia CA. A new approach to free vibration analysis using boundary elements. Appl Math Model 1983;7(3):157–62.
[11] Kansa EJ. Multiquadrics—a scattered data approximation scheme with applications to computational fluid-dynamics. I. Surface approximations and partial derivative estimates. Comput Math Appl 1990;19(8/9):127–45.
[12] Kansa EJ. Multiquadrics—a scattered data approximation scheme with applications to computational fluid-dynamics. II. Solutions to hyperbolic, parabolic and elliptic partial differential equations. Comput Math Appl 1990;19:147–61.
[13] Driscoll TA, Fornberg B. Interpolation in the limit of increasingly flat radial basis functions. Comput Math Appl 2002;43(3):413–22.
[14] Ferreira AJM. A formulation of the multiquadric radial basis function method for the analysis of laminated composite plates. Compos Struct 2003;59(3):385–92.
[15] Ferreira AJM, Roque CMC, Martins PALS. Radial basis functions and higher-order shear deformation theories in the analysis of laminated composite beams and plates. Compos Struct 2004;66(1–4):287–93.
[16] Ferreira AJM. Polyharmonic (thin-plate) splines in the analysis of composite plates. Int J Mech Sci 2005;46(3):1549–69.
[17] Ferreira AJM, Roque CMC, Jorge RMN. Free vibration analysis of symmetric laminated composite plates by FSDT and radial basis functions. Comput Meth Appl Mech Eng 2005;194(39–41):4265–78.
[18] Larsson E, Fornberg B. Theoretical and computational aspects of multivariate interpolation with increasingly flat radial basis functions. Comput Math Appl 2005;49:103–30.

[19] Rippa S. An algorithm for selecting a good value for the parameter *c* in radial basis function interpolation. Adv Comput Math 1999;11(2–3):193–210.
[20] Wertz J, Kansa EJ, Ling L. The role of the multiquadric shape parameters in solving elliptic partial differential equations. Comput Math Appl 2006;51(8): 1335–48.
[21] Naffa M, Al-Gahtani H. RBF-based mesh-less method for thin plates undergoing large deformations. Eng Anal Bound Elements 2007;31(4):311–7.
[22] Librescu L. The elastostatic and kinetics of anisotropic and heterogeneous shell-type structures. Leiden: Noordhoff; 1975.
[23] ANSYS 9.0, ANSYS documentation, 2005.